Journal of Molecular Structure 1299 (2024) 137114

Contents lists available at ScienceDirect

Journal of Molecular Structure

journal homepage: www.elsevier.com/locate/molstr

Modular symmetric ligands for selective recognition of cancer-relevant G-quadruplexes

Chiara Platella [a,1], Andrea Citarella [b,1], Marco Manenti [b], Guglielmo Spinelli [b], Rosa Gaglione [a], Angela Arciello [a], Claudia Riccardi [a], Domenica Musumeci [a,c], Daniela Montesarchio [a,*], Clelia Giannini [b,*], Alessandra Silvani [b]

[a] Department of Chemical Sciences, University of Naples Federico II, via Cintia 21, 80126 Napoli, Italy
[b] Department of Chemistry, University of Milan, Via Golgi 19, 20133 Milano, Italy
[c] Institute of Biostructures and Bioimages, IBB-CNR, via Tommaso De Amicis 95, 80145 Napoli, Italy

ARTICLE INFO

Keywords:
G-quadruplex
Ligand design
Symmetric ligands
Oxazole

ABSTRACT

New G-quadruplex-interactive and selective ligands are strongly required to evolve innovative, effective and minimally toxic anticancer agents. With this purpose, we have here synthesized and evaluated a mini-library of organic molecules featured by aromatic cores of different rigidity (naphthalene or bioxazole), decorated with pendant groups including positively charged moieties and/or H-bond donors/acceptors. By exploiting different biophysical techniques, we proved the ability of the bioxazole-based derivatives to strongly and selectively interact with telomeric and oncogenic G-quadruplexes, while the compound featured by a naphthalene core did not emerge as a good G-quadruplex ligand. Molecular docking studies demonstrated the ability of the bioxazole-based ligands to preferentially target the outer G-tetrads of both telomeric and oncogenic G-quadruplexes, by positioning their cores on the G-tetrads in a symmetrical or asymmetrical way respectively, with the pendant groups pointing towards or away from the grooves. All bioxazole-based ligands showed anticancer activity in the low micromolar range. Particularly, the bioxazole derivative bearing piperazine groups was the most active compound of the investigated series, whereas the derivatives bearing morpholine groups were the most selective ones on cancer cells, in full agreement with their ability to act as the strongest and most selective G-quadruplex ligands, respectively.

1. Introduction

Cancer is one of the leading causes of death in the world with more than 10 million mortalities annually. Current cancer treatments comprise surgical intervention, radiation and chemotherapeutic drugs [1]. However, side effects are typically associated to these treatments. Therefore, current studies focus on the search for new strategies that significantly reduce any undesirable side effect [1,2].

In this frame, non-canonical structures of nucleic acids, such as G-quadruplexes, have attracted great attention for their involvement in various and specific cancer-related biological processes [3]. Particularly, G-quadruplexes can be formed in G-rich regions of DNA and RNA, and consist of cyclic, planar arrangements of four guanines – held together by Hoogsteen-type H-bonds – called G-tetrads, which are stacked one on top of the other, generating a central cavity typically hosting metal cations. The sequences connecting the tracts of adjacent guanines are called loops [4]. G-quadruplexes exhibit high structural polymorphism depending on the number and relative orientation of involved strands, type of loops, guanine residues conformation and nature of the associated metal cations [4].

G-quadruplex structures play crucial roles in the regulation of telomerase activity and expression of oncogenes at the transcriptional and translational levels. Therefore, their stabilization by specific ligands has been recognized as a promising strategy for anticancer therapy [5–7].

In general, G-quadruplex ligands are small molecules that can bind this kind of structures in a variety of ways, including stacking on external G-tetrads, loops/grooves binding or binding to both G-tetrads and loops/grooves. Accordingly, G-quadruplex ligands share a number

* Corresponding authors.
E-mail addresses: daniela.montesarchio@unina.it (D. Montesarchio), clelia.giannini@unimi.it (C. Giannini).
[1] These authors equally contributed to the work.

https://doi.org/10.1016/j.molstruc.2023.137114
Received 27 July 2023; Received in revised form 2 October 2023; Accepted 17 November 2023
Available online 22 November 2023

of common structural features, such as polycyclic heteroaromatic cores that can target the external G-tetrads, and polar or positively charged hydrophilic groups that can facilitate binding to G-quadruplex loops/grooves [8,9].

Over the past two decades a large number of organic small molecules has been synthesized and proved to bind to DNA/RNA G-quadruplexes [10–15]. Among them, three main groups sharing common structural features emerged, namely fused aromatic polycyclic systems (e.g., **BRACO-19** [16] and **TT-Gn$_3$** [17]), macrocycles (e.g., **TMPyP4** [18] and **L2H2-6M(2)OTD** [19]) and not fully fused aromatic systems (e.g., **DIZ-3** [20] and **TOxaPy** [21]).

The latter class of molecules, also called modular G-quadruplex ligands, seems to be the most promising one. Indeed, modular ligands are featured by aromatic modules combined to create flexible structural motifs, potentially able to selectively recognize G-quadruplex structures and discriminate among the different G-quadruplex topologies, by targeting not only the terminal G-tetrads but also loops and grooves.

Although many of the already described compounds display high affinity for G-quadruplexes, they often recognize their target via a non-specific binding mode. Furthermore, most of them do not possess drug-like properties, e.g. they do not satisfy Lipinski's rule of five and do not exhibit favorable ADMET profiles [22]. For these reasons, in parallel with deeper investigations on the mechanisms and biological effects of the existing most promising G-quadruplex ligands, it is of the utmost importance to reinforce the research on the design and synthesis of new G-quadruplex-interactive and selective ligands. Indeed, to increase the affinity of ligands for G-quadruplexes and the specificity over duplex DNA, further modifications of their chemical structures and molecular properties are necessary.

In this context, aiming at discovering novel potential anticancer agents, we have synthesized and evaluated a small library of organic molecules as putative and selective ligands of telomeric and oncogenic G-quadruplexes. The target compounds share some common structural features, such as modularity, symmetry, and presence of two basic residues useful for the interaction with nucleotide phosphate groups. More precisely, these residues were selected based on their different basicity, as well as their capacity to be involved in H-bond interactions.

As telomeric and oncogenic G-quadruplexes, the tel26 sequence, taken from the human telomere, and the c-myc/pu22 sequences, taken from the human oncogenic promoter *c-myc*, able to form unimolecular hybrid and parallel G-quadruplexes respectively, were chosen as models for affinity evaluation [23,24]. In parallel, in order to evaluate the selectivity of G-quadruplex recognition, the Dickerson sequence, able to form a B-DNA duplex structure, was used as control [25].

The binding of the newly synthesized molecules with the DNA models was investigated by multiple biophysical techniques in a combined approach. In detail, the G-quadruplex on Controlled Pore Glass (G4-CPG) assay [26] – a cheap and easy affinity chromatography-based method recently developed by our research group – was exploited to assess the capacity of the examined synthetic compounds to interact with G-quadruplexes, as well as their G-quadruplex vs. duplex selectivity. Then, these compounds were tested for their ability to affect the conformation and/or thermally stabilize the target G-quadruplex structures by circular dichroism (CD), using the duplex model as control. Fluorescence spectroscopy titrations were exploited to study the interaction of the fluorescent ligands with the DNA models and determine their binding constants. Further insight into the binding mode of the compounds to the G-quadruplex models was obtained by molecular docking. Finally, the studied compounds were tested for their anticancer activity on different cancer cell lines, using normal cells as controls.

2. Results and discussion

2.1. Design and synthesis of potential G-quadruplex ligands

The bicyclic naphthalene framework was chosen as the first central core to design our target compounds. The synthesis of **GS1** was pursued starting from the commercially available 2,7-dibromonaphtalene, which was readily converted into the corresponding naphthalene-2,7-dicarbaldehyde **1** *via* formylation (Scheme 1) [27]. Then, the modular target compound was obtained in moderate yield exploiting the multicomponent Van Leusen reaction of 1,4-(2-aminoethyl) morpholine and toluenesulfonylmethyl isocyanide (TosMIC).

To evaluate the role of the central core and in particular its rigidity, more flexible target compounds with a central 2,2′-bioxazole core were also designed. In this case, starting compound was the already known compound **2**, which underwent oxidative C-C homocoupling [28] to afford the symmetric intermediate **3**. We were pleased to observe that the formyl group, even though not protected, did not interfere with the smooth course of the Pd-catalyzed reaction.

The two formyl groups in intermediate **3** were subjected to different transformations, aimed at introducing basic side arm substituents useful to form electrostatic and H-bond interactions with the loops/grooves of the G-quadruplexes. First, compound **3** was reacted with aminoguanidine hydrochloride under acidic conditions, affording the weakly basic bis-guanylhydrazone **GS2**, as hydrochloride salt. The guanylhydrazones represent an emerging class of compounds, endowed with a great variety of biological activities and featuring a significant BBB-permeability at physiological pH.

Then, the diformyl derivative **3** was converted - exploiting a reductive amination, using two different amines, namely 4-(2-aminoethyl) morpholine and 2-(4-methyl-piperazin-1-yl)-ethylamine - into the target compounds **GS3** and **GS4**. Applying the same overall strategy, the pyridine analogue **GS5** was also obtained, starting from the known substrate **4**. After purification, all the final compounds were fully characterized by ^{1}H NMR, ^{13}C NMR, IR and HR-MS (see Materials and methods and Supporting Information).

2.2. Evaluation of the synthesized compounds by the G4-CPG assay

The synthesized compounds were then preliminarily tested in their ability to bind to G-quadruplex structures using the G4-CPG assay. This assay consists in flowing solutions of potential ligands through Controlled Pore Glass (CPG) beads functionalized with a G-quadruplex-forming oligonucleotide. The compounds with high affinity for the G-quadruplex are retained, while those with low-to-null affinity are rapidly eluted. All the steps of this assay are monitored by simple UV measurements [26,29,30].

In detail, the following cancer-related G-quadruplex-forming DNA sequences were chosen as the targets of interest:

- tel26, a 26-mer oligonucleotide, able to fold into a hybrid G-quadruplex in intracellular-mimicking buffer conditions, with sequence d(TTAGGGTTAGGGTTAGGGTTAGGGTT) extracted from the human 3′-telomeric overhang, i.e. the telomerase natural target; [31]
- c-myc, a 33-mer oligonucleotide, able to fold into a parallel G-quadruplex, with sequence d(TGGGGAGGGTGGGGAGGGTGGGGAAGGTGGGGA) extracted from the regulatory region of the gene coding for the transcription factor C-MYC [32].

All the experiments carried out on the G-quadruplex targets were also performed in parallel on a 27-mer unimolecular duplex-forming DNA sequence, hereafter named ds27, to determine if the analyzed compounds can discriminate G-quadruplex vs. duplex DNA. In particular, the duplex of choice consists of two self-complementary tracts, each containing the Dickerson sequence d(CGCGAATTCGCG), i.e. one of the best studied models for B-DNA [25], connected by a TTT loop.

The stock solutions of the naphthalene- and bioxazole-based derivatives were prepared by dissolving the solid compounds in pure DMSO. Then, the solubility and stability of the tested compounds were evaluated at the concentration and in the washing/releasing solutions used in the G4-CPG assay. All these compounds proved to be fully

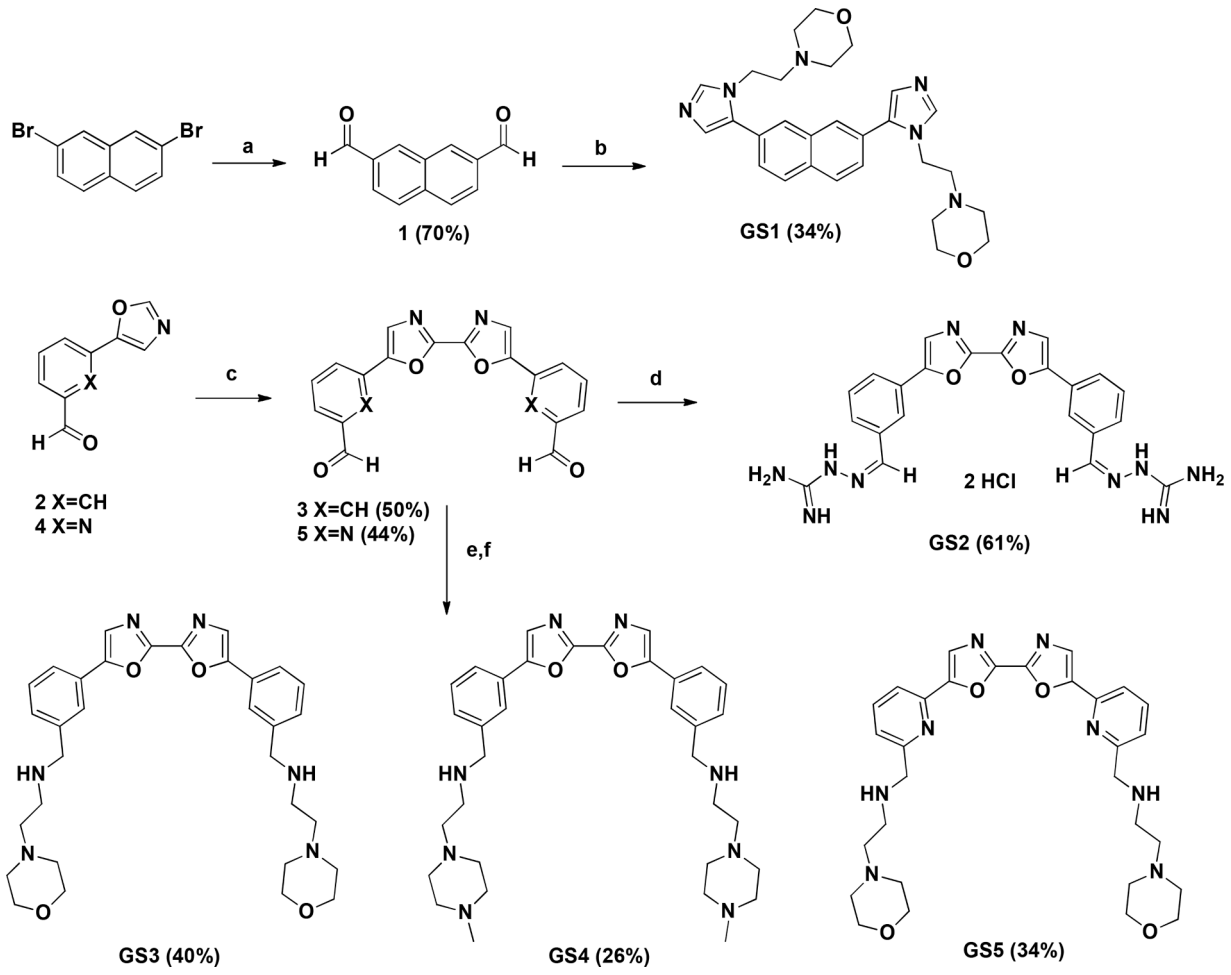

Scheme 1. Reagents and conditions: a) n-BuLi, DMF, THF, −78 °C to r.t.; b) 4-(2-aminoethyl) morpholine, K_2CO_3, TosMIC, MeOH/DMF, reflux; c) $Pd(OAc)_2$, Ph_3P, CuCl, $Cu(OAc)_2$, 1,4-dioxane/DMSO, reflux; d) aminoguanidine hydrochloride, EtOH, 1 M HCl, reflux; e) appropriate amine, MeOH, reflux; f) $NaBH_4$, MeOH, reflux; for details see Materials and methods.

soluble and stable in the assay experimental conditions. For each of the five compounds here synthesized, tests were carried out to evaluate first the unspecific binding on nude CPG support, and then the ability to bind G-quadruplexes- and duplex-forming DNA oligonucleotide sequences. The results of the G4-CPG assays are summarized in Table 1. Generally, no significant unspecific binding was observed, thus not precluding their further analyses on the oligonucleotide-functionalized supports.

Table 1
Summary of the binding assay data obtained for the five synthetic compounds as determined by the G4-CPG assay. The amounts of bound ligand are calculated as a difference between the initially loaded amount of ligand and the unbound ligand, recovered by the washing solution (50 mM KCl, 10% DMSO, 10% CH_3CH_2OH), and are expressed as percentage of the quantity initially loaded on each support. The errors associated with the reported percentages are typically within ±2%. The selectivity index is the ratio between the percentages of ligand bound to the indicated supports.

Compound	Bound ligand (%)				Selectivity index		
	Nude CPG	CPG-tel26	CPG-c-myc	CPG-ds27	CPG-tel26/CPG-ds27	CPG-c-myc/CPG-ds27	CPG-c-myc/CPG-tel26
GS1	0	7	8	12	0.58	0.67	1.1
GS2	0	78	87	85	0.92	1.0	1.1
GS3	0	54	57	51	1.1	1.1	1.1
GS4	0	66	75	68	0.97	1.1	1.1
GS5	6	41	59	29	1.4	2.0	1.4

Overall, with the only exception of **GS1**, all compounds showed a remarkable ability to interact with G-quadruplex-functionalized supports, especially **GS2** and **GS4**. In detail, from the acquired data the following affinity order was obtained for the hybrid G-quadruplex tel26: **GS2** > **GS4** > **GS3** > **GS5** > **GS1**. In parallel, the following affinity order for the parallel G-quadruplex c-myc was obtained: **GS2** > **GS4** > **GS5** > **GS3** > **GS1**.

Furthermore, to evaluate the ability of each ligand to discriminate between G-quadruplex and duplex structures, a selectivity index was determined based on the ratio between the percentage of ligand bound to the G-quadruplex models and the one bound to the control duplex (Table 1). The order of selectivity, going from the most selective to the least selective compound for the hybrid G-quadruplex tel26, was: **GS5** > **GS3** > **GS4** > **GS2** > **GS1**, whereas for the parallel G-quadruplex c-myc was: **GS5** >> **GS3** = **GS4** > **GS2** > **GS1**. In parallel, the ability of the compounds to selectively recognize a specific G-quadruplex topology was evaluated by calculating the ratio between the percentage of ligand bound to the parallel G-quadruplex c-myc and the ligand bound to the hybrid G-quadruplex tel26. Interestingly, all compounds showed a slight preference for the parallel G-quadruplex c-myc.

2.3. Solution studies on the interaction of the synthesized compounds with G-quadruplex models and a control duplex

In addition to the G4-CPG assay, the ability of the here synthesized compounds to interact with the G-quadruplex models and the control

duplex was also evaluated by in-solution biophysical characterization techniques, i.e. CD and fluorescence spectroscopy. The oligonucleotide models for the human telomeric G-quadruplex and the control duplex were the same as used in the G4-CPG assay, i.e. the sequence d(TTAGGGTTAGGGTTAGGGTTAGGGTT), named tel26, and the self-complementary Dickerson dodecamer d(CGCGAATTCGCG), hereafter named ds12, respectively. On the other hand, considering that the c-myc sequence is characterized by the coexistence of multiple parallel G-quadruplexes in equilibrium [33] and thus does not represent a good model for semi-quantitative solution studies, one of its shorter variants of sequence d(TGAGGGTGGGTAGGGTGGGTAA), hereafter named pu22, was selected for our study, being featured by a single major conformation.

2.3.1. CD titration and melting experiments

As far as the CD experiments are concerned, the G-quadruplex-forming oligonucleotides, as well as the control duplex, were prepared by annealing the DNA solutions at 2 μM concentration, in 20 mM KCl, 5 mM potassium phosphate buffer (pH 7) for tel26 and ds12 or 10 mM Tris–HCl buffer (pH 7) for pu22.

According to the literature, under these conditions the analyzed sequences adopted the following conformations, as indicated by their CD profiles (Figure S1, left panels):

- tel26 folded into a hybrid 2-type G-quadruplex, featured by a positive CD band with maximum centered at 290 nm and a shoulder at 270 nm; [34]
- pu22 exhibited a positive band centered at 263 nm and a negative one with minimum at 240 nm, typical of a parallel G-quadruplex; [24]
- ds12 showed a positive band at 281 nm along with a negative one with minimum at 253 nm, characteristic of a B-DNA duplex structure [35,36].

The three oligonucleotides were titrated with increasing amounts (up to 2 molar equivalents) of each compound, and the corresponding CD spectra were recorded after each addition (Figures S2 and 1–4, left panels).

CD titration experiments of tel26 showed: i) a dose-dependent increase of the 290 nm band accompanied by a reduction of the 270 nm shoulder intensity for **GS2** (Fig. 1); ii) a dose-dependent reduction of the 270 nm shoulder intensity for **GS3, GS4** and **GS5** (Figs. 2-4); iii) no relevant changes of the G-quadruplex conformation upon treatment with **GS1** (Figure S2). Interestingly, the appearance of an additional shoulder at ca. 250 nm was observed in the case of tel26 titration with **GS2, GS3** and **GS4** (Figs. 1–3), suggesting a conformational conversion of the tel26 G-quadruplex from hybrid 2 to hybrid 1 topology [31,37].

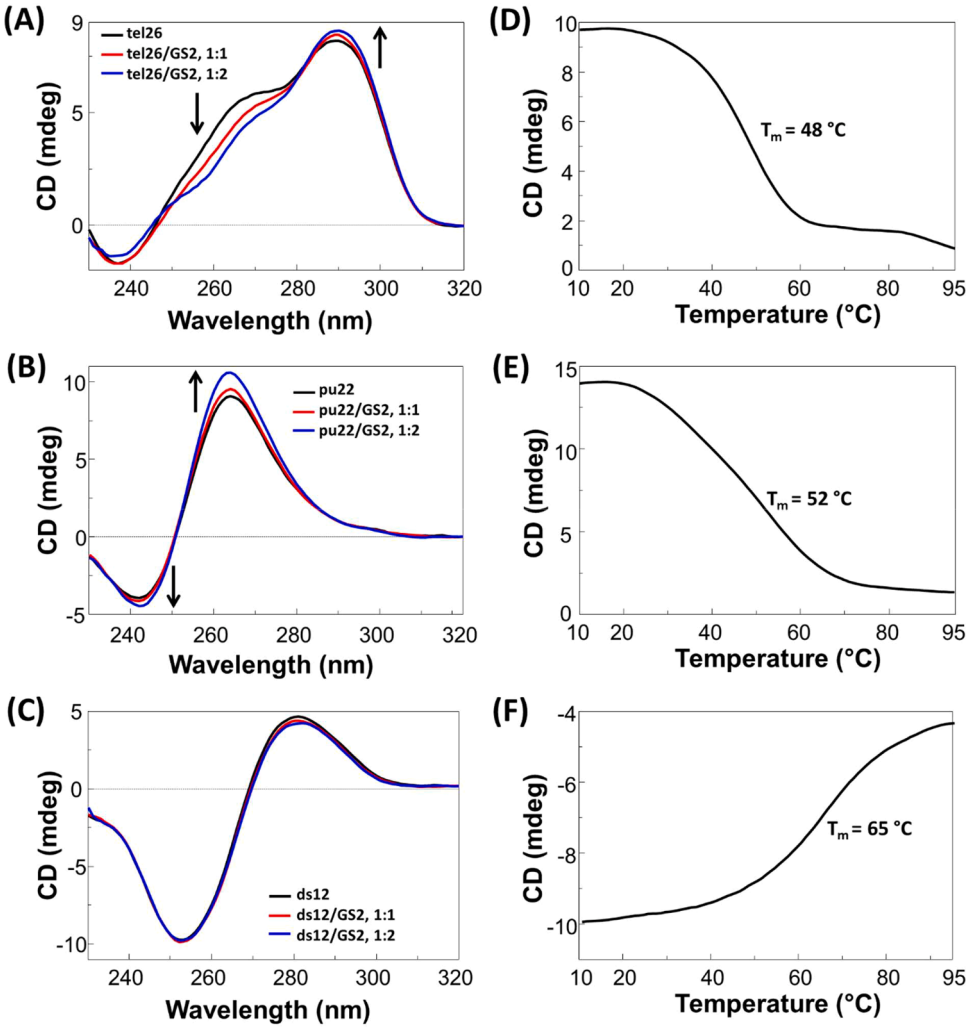

Fig. 1. Left panels: CD spectra of 2 μM solutions of tel26 (A), pu22 (B) and ds12 (C) in 20 mM KCl, 5 mM potassium phosphate buffer (pH 7) for tel26 and ds12 or in 10 mM Tris–HCl buffer (pH 7) for pu22 in the presence of increasing amounts (up to 2 equivalents) of **GS2**. Arrows indicate the variation of CD bands on increasing ligand concentration. Right panels: CD melting curves for tel26 (D), pu22 (E) and ds12 (F) in the presence of **GS2** (2 equivalents) in 20 mM KCl, 5 mM potassium phosphate buffer (pH 7) for tel26 and ds12, recorded at 290 and 253 nm respectively, and in 10 mM Tris–HCl buffer (pH 7) for pu22, recorded at 263 nm.

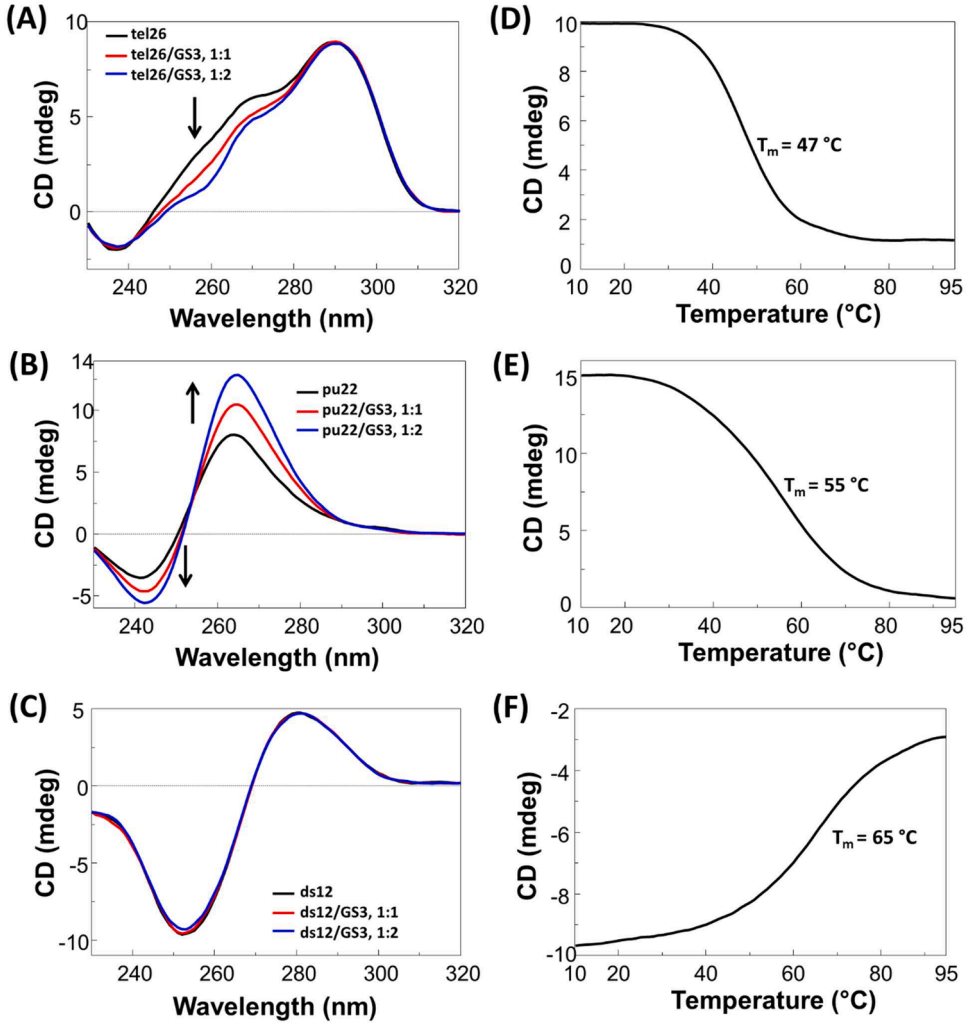

Fig. 2. Left panels: CD spectra of 2 μM solutions of tel26 (A), pu22 (B) and ds12 (C) in 20 mM KCl, 5 mM potassium phosphate buffer (pH 7) for tel26 and ds12 or in 10 mM Tris–HCl buffer (pH 7) for pu22 in the presence of increasing amounts (up to 2 equivalents) of **GS3**. Arrows indicate the variation of CD bands on increasing ligand concentration. Right panels: CD melting curves for tel26 (D), pu22 (E) and ds12 (F) in the presence of **GS3** (2 equivalents) in 20 mM KCl, 5 mM potassium phosphate buffer (pH 7) for tel26 and ds12, recorded at 290 and 253 nm respectively, and in 10 mM Tris–HCl buffer (pH 7) for pu22, recorded at 263 nm.

As far as the CD titration experiments of pu22 are concerned, a dose-dependent increase of the intensity of both the 263 and 240 nm bands was observed for all compounds, with the sole exception of **GS1**, which did not significantly affect the pu22 G-quadruplex conformation (Figs. S2 and 1–4).

Notably, no detectable changes in the CD profile of the control duplex were observed for all the investigated compounds (Figs. S2 and 1, 2 and 4), if not a slight reduction of the intensity of the 253 nm band for **GS4** (Fig. 3).

In parallel, the DNA-stabilizing (or destabilizing) properties of all the tested compounds were evaluated by CD melting experiments on all DNA/ligand mixtures, by measuring the ligand-induced change in the melting temperature (ΔT_m) of the G-quadruplex models and the control duplex. CD melting curves of tel26, pu22 and ds12 in the absence or presence of each ligand (DNA/ligand 1:2 ratio) were recorded by following the CD changes at the wavelength of the intensity maximum or minimum (290, 263 and 253 nm for tel26, pu22 and ds12, respectively).

Melting temperatures (T_m) of 43, 27 and 65 °C were found for free tel26, pu22 and ds12, respectively (Fig. S1, right panels). The T_m and ΔT_m values for all the studied DNA/ligand systems (Figs. S2 and 1–4, right panels) are summarized in Table 2.

Strong stabilizing effects were detected for all compounds, except for **GS1**, on both tel26 and pu22 G-quadruplexes. In detail, ΔT_m values in the range +3 - +5 °C and +23 - +28 °C were found in the case of tel26 and pu22, respectively. In contrast, no stabilization on the control duplex was observed for all the tested compounds ($\Delta T_m = 0$ or +1 °C).

Taken together, these results demonstrated the ability of the here investigated compounds, apart from **GS1**, to selectively interact with the telomeric and oncogenic G-quadruplex models, in full agreement with the G4-CPG assay results, showing strong stabilizing effect on both tel26 and especially pu22 G-quadruplexes but not on the control duplex.

2.3.2. *Fluorescence spectroscopy studies*

In order to study more in detail DNA/ligand interactions, fluorescence spectroscopy titrations were performed for the synthetic compounds of the investigated series showing a stable fluorescence spectrum over time, i.e. **GS3, GS4** and **GS5**.

Titrations were performed at a fixed concentration (2.0 μM) of ligand by adding increasing amounts of tel26, pu22 and ds12 (up to 5 μM). Then, the fraction of bound ligand was calculated from the fluorescence intensity values obtained and plotted as a function of DNA concentration. These data were then fitted with an independent and equivalent site model [38] to calculate the binding constant (K_b) values.

Significant fluorescence quenching was observed upon titration of **GS3, GS4** and **GS5** with all three oligonucleotides, but was less marked in the case of the control duplex (Figs. 5–7, left panels). The fitting

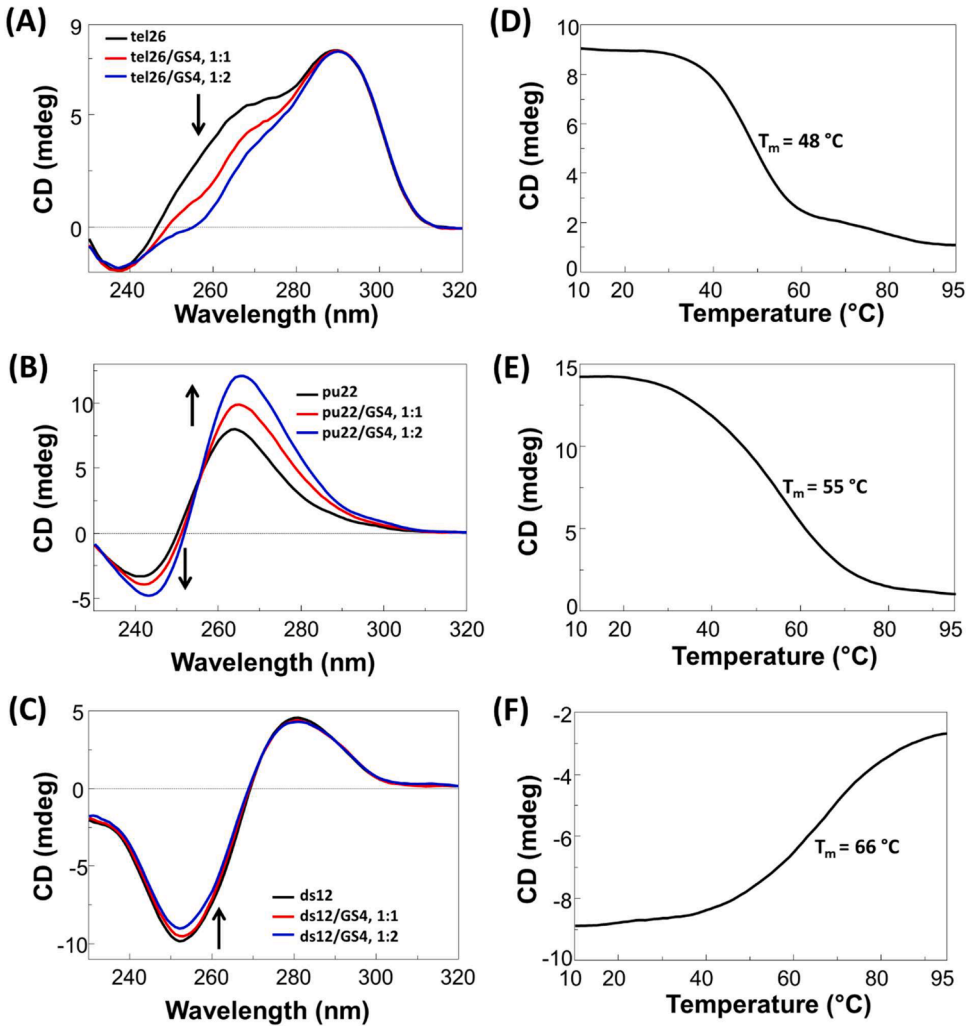

Fig. 3. Left panels: CD spectra of 2 μM solutions of tel26 (A), pu22 (B) and ds12 (C) in 20 mM KCl, 5 mM potassium phosphate buffer (pH 7) for tel26 and ds12 or in 10 mM Tris–HCl buffer (pH 7) for pu22 in the presence of increasing amounts (up to 2 equivalents) of **GS4**. Arrows indicate the variation of CD bands on increasing ligand concentration. Right panels: CD melting curves for tel26 (D), pu22 (E) and ds12 (F) in the presence of **GS4** (2 equivalents) in 20 mM KCl, 5 mM potassium phosphate buffer (pH 7) for tel26 and ds12, recorded at 290 and 253 nm respectively, and in 10 mM Tris–HCl buffer (pH 7) for pu22, recorded at 263 nm.

curves related to the fluorescence data of **GS3, GS4** and **GS5** with tel26 and pu22 G-quadruplexes and ds12 duplex are shown in Figs. 5–7 (right panels), whereas the K_b values for all the studied DNA/ligand systems are summarized in Table 3.

From the obtained K_b values, **GS4** emerged as the strongest ligand of tel26 and pu22 G-quadruplexes ($K_b = 5.8 \pm 1.8 \times 10^6$ M^{-1} and $8.4 \pm 2.3 \times 10^6$ M^{-1}, respectively), showing a preference for the parallel G-quadruplex pu22. However, considering the value of the binding constant with ds12 control duplex ($K_b = 2.3 \pm 1.0 \times 10^6$ M^{-1}), even if a good G-quadruplex vs. duplex selectivity was observed, **GS4** proved to be the least selective ligand in the series according to the fluorescence spectroscopy data. In turn, **GS3** showed a higher affinity for the hybrid G-quadruplex tel26 ($K_b = 5.3 \pm 1.8 \times 10^6$ M^{-1}) than for the parallel G-quadruplex pu22 ($K_b = 1.7 \pm 0.5 \times 10^6$ M^{-1}), whereas **GS5** was found to be a stronger ligand of pu22 ($K_b = 5.1 \pm 1.8 \times 10^6$ M^{-1}) than of tel26 ($K_b = 2.8 \pm 0.8 \times 10^6$ M^{-1}). Moreover, on comparing **GS3** and **GS5**, the most selective ligand for G-quadruplexes vs. duplex DNA was **GS5**, showing a lower K_b value for the control duplex ($K_b = 2.1 \pm 0.3 \times 10^5$ M^{-1}) compared to **GS3** ($K_b = 4.4 \pm 0.4 \times 10^5$ M^{-1}).

Notably, both the affinity and selectivity values observed by fluorescence titrations for the three ligands towards the three model oligonucleotides showed the same trend as observed in the G4-CPG assay. Altogether these data further corroborated these compounds as strong and selective ligands of G-quadruplexes, in full agreement with the G4-CPG assay and CD results.

2.4. Docking studies

To get a deeper insight into the binding mode of the new G-quadruplex ligands here identified, i.e. **GS2, GS3, GS4** and **GS5**, to tel26 and pu22 G-quadruplexes, molecular docking studies were carried out in order to build structural models for the 1:1 DNA/ligand complexes.

All ligands preferentially targeted the outer G-tetrads of both the hybrid tel26 and parallel pu22 G-quadruplexes (Fig. 8). In detail, the cores of all four ligands were centered on the top of the outer G-tetrad in the case of pu22 G-quadruplex (Fig. 8E–H), while the cores were stacked only on two of the four guanines involved in the outer G-tetrad of tel26 G-quadruplex (Fig. 8A–D). The two oxazole rings of the core of the ligands adopted an almost planar arrangement when bound to tel26 and pu22 G-quadruplexes, with the only exception of the interaction of **GS2** and **GS4** with tel26 G-quadruplex, in which the two oxazole rings were perpendicular to each other.

As far as the two pendant groups of each ligand are concerned, only one of them pointed to (for **GS4**) or was inserted into (for **GS2, GS3** and **GS5**) the tel26 G-quadruplex groove, while the other one was directed towards the outer G-tetrad (Fig. 8A–D). On the other hand, the pendant

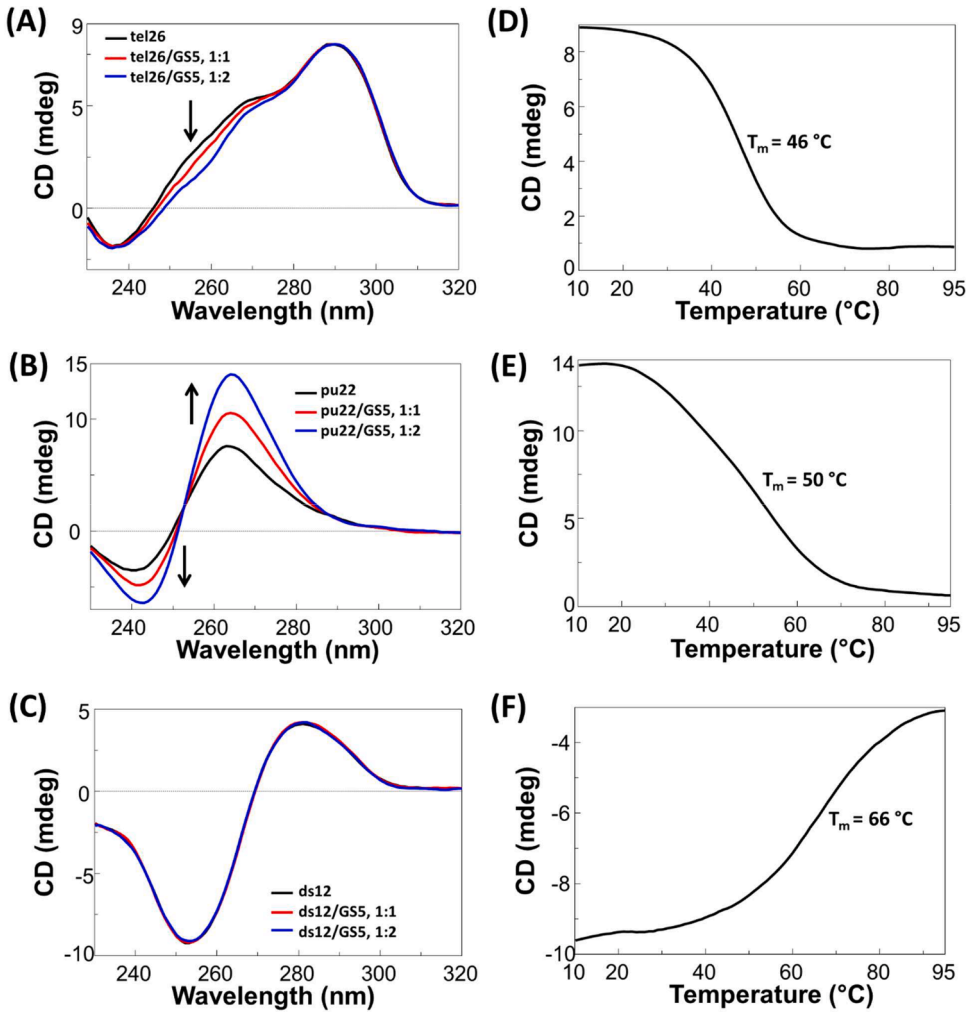

Fig. 4. Left panels: CD spectra of 2 μM solutions of tel26 (A), pu22 (B) and ds12 (C) in 20 mM KCl, 5 mM potassium phosphate buffer (pH 7) for tel26 and ds12 or in 10 mM Tris–HCl buffer (pH 7) for pu22 in the presence of increasing amounts (up to 2 equivalents) of **GS5**. Arrows indicate the variation of CD bands on increasing ligand concentration. Right panels: CD melting curves for tel26 (D), pu22 (E) and ds12 (F) in the presence of **GS5** (2 equivalents) in 20 mM KCl, 5 mM potassium phosphate buffer (pH 7) for tel26 and ds12, recorded at 290 and 253 nm respectively, and in 10 mM Tris–HCl buffer (pH 7) for pu22, recorded at 263 nm.

Table 2
Melting temperature (T_m) values of tel26, pu22 and ds12 in the presence of the investigated compounds (2 molar equivalents) as measured by CD melting experiments in 20 mM KCl, 5 mM potassium phosphate buffer (pH 7) for tel26 and ds12 or 10 mM Tris–HCl buffer (pH 7) for pu22. $\Delta T_m = T_m$(DNA/ligand, 1:2) - T_m(free DNA).

Compound	tel26		pu22		ds12	
	$T_m \pm 1$ (°C)	ΔT_m (°C)	$T_m \pm 1$ (°C)	ΔT_m (°C)	$T_m \pm 1$ (°C)	ΔT_m (°C)
GS1	43	0	28	+1	65	0
GS2	48	+5	52	+25	65	0
GS3	47	+4	55	+28	65	0
GS4	48	+5	55	+28	66	+1
GS5	46	+3	50	+23	66	+1

groups pointed both away (for **GS2** and **GS4**) from the pu22 G-quadruplex groove (Fig. 8E,G) or were both inserted (for **GS3** and **GS5**) into the groove (Fig. 8F,H).

Overall, the asymmetrical position of the ligand cores stacked on the tel26 G-tetrad allowed maximizing the interactions of one of the two pendant groups with the grooves, while in the symmetrical position of the ligand cores on the pu22 G-tetrad both the substituents were close to the grooves with their interactions averaged. Finally, the morpholine groups appeared to be deeper accommodated in the grooves than guanyl hydrazone or piperazine groups.

2.5. *Biological assays*

The cytotoxic activity of the here investigated compounds was evaluated by performing MTT assays on human HeLa adenocarcinoma cells, human MCF7 breast cancer cells, and on human HaCaT keratinocytes selected as control normal cells. As reported in Fig. S3, all the compounds were endowed with significant dose-dependent antiproliferative effects upon incubation with the tested cell lines.

From an overall inspection of the cellular data, **GS1** proved to be the least active species, showing the lowest antiproliferative activity compared to all other compounds on all the tested cell lines (IC_{50} values of 41, 32 and 35 μM at 72 h incubation for HeLa, MCF7 and HaCaT, respectively, Table 4). On the other hand, the strongest antiproliferative effects were detected for **GS4**, showing IC_{50} values in the range 5–12 μM at 72 h. Under the same conditions, **GS2, GS3** and **GS5** evidenced antiproliferative effects with IC_{50} values comprised between 21 and 24, 20–23 and 25–42 μM, respectively. Thus, a good correlation between the antiproliferative activity of **GS2, GS3, GS4** and **GS5** and their ability to target telomeric and oncogenic G-quadruplexes was evidenced, well reproducing the trend observed with the G4-CPG assay and the spectroscopic data.

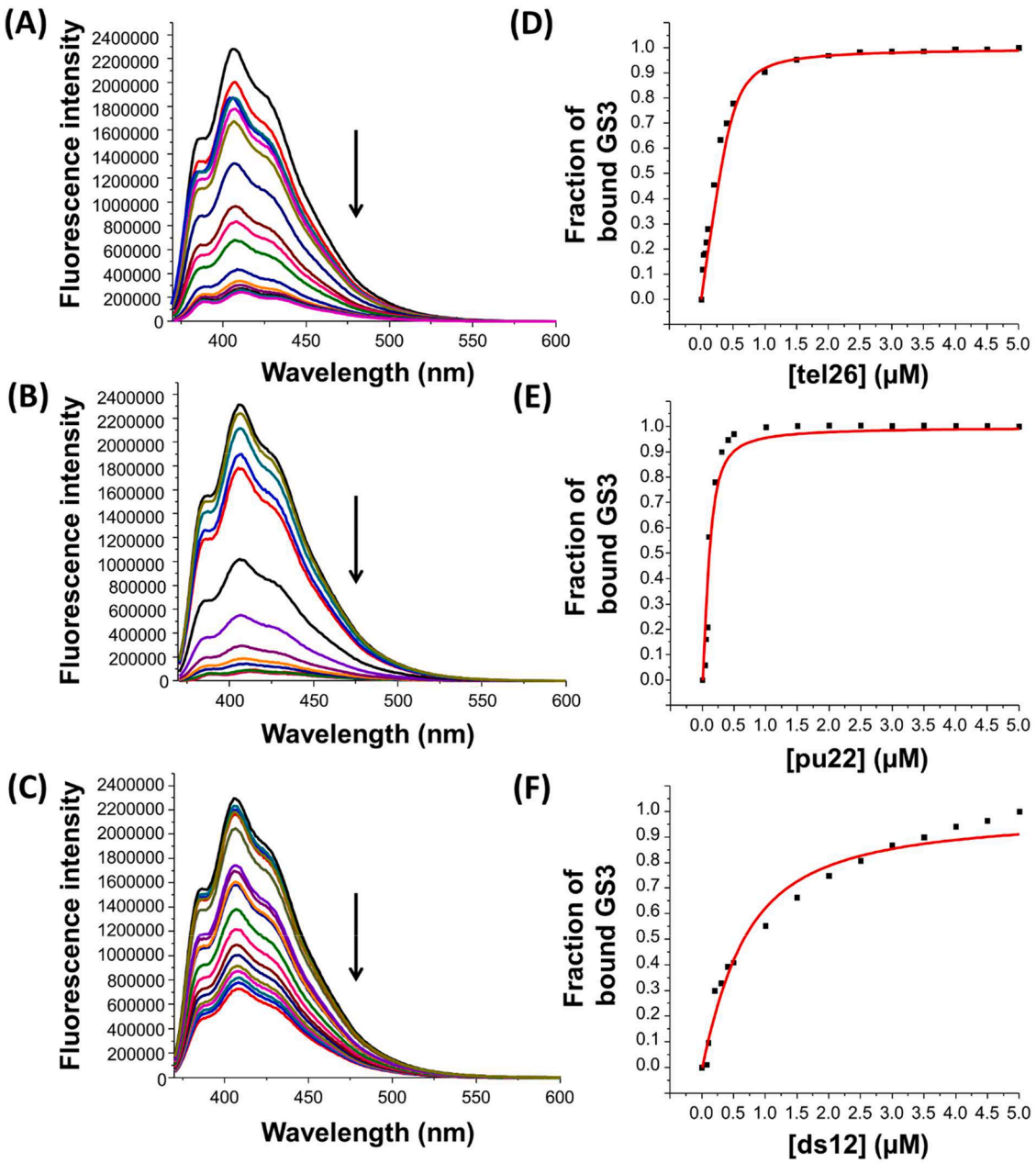

Fig. 5. Left panels: Fluorescence spectra obtained by adding increasing amounts of tel26 (A), pu22 (B) and ds12 (C) to solutions at a fixed concentration of **GS3** (2 μM). Arrows indicate the variation of fluorescence intensity on increasing DNA concentration. Right panels: Representative binding curves obtained by plotting the fraction of bound **GS3** to tel26 (D), pu22 (E) and ds12 (F) as a function of DNA concentration. The black squares represent experimental data; the red line represents the best fit obtained using an independent and equivalent-site model.

3. Conclusions

Aim of this work was the identification of novel compounds able to specifically recognize the G-quadruplex structures of human telomere and c-myc oncogene promoter in the context of the development of new effective and minimally toxic anticancer drugs [26].

To this purpose, a mini-library of novel organic compounds, including naphthalene- (**GS1**) and bioxazole-based (**GS2, GS3, GS4** and **GS5**) derivatives, was designed, synthesized, and characterized. All these compounds contained an aromatic core of different rigidity, decorated with pendant groups including positively charged moieties and/or H-bond donors/acceptors. The interaction of these molecules with telomeric and oncogenic G-quadruplex structures was investigated by multiple biophysical techniques, *i.e.* the G4-CPG assay [26], CD and fluorescence spectroscopy, using a duplex structure as selectivity control.

In detail, the G4-CPG assay was exploited to preliminarily assess the capacity of the examined synthetic compounds to interact with G-quadruplexes, as well as their G-quadruplex *vs.* duplex selectivity. With the only exception of **GS1**, all compounds showed a remarkable ability to interact with the telomeric and oncogenic G-quadruplexes, as well as a good ability to discriminate between the G-quadruplex models and the control duplex.

Furthermore, the compounds were tested for their ability to affect and/or thermally stabilize the G-quadruplex structures by CD analysis. Except for **GS1**, all compounds showed strong stabilizing effects on both telomeric and oncogenic G-quadruplexes by CD titration experiments. Notably, in the case of tel26 titration with **GS2, GS3** and **GS4**, a conformational switch of the tel26 G-quadruplex from hybrid 2 to hybrid 1 topology was found upon interaction with the ligands. On the

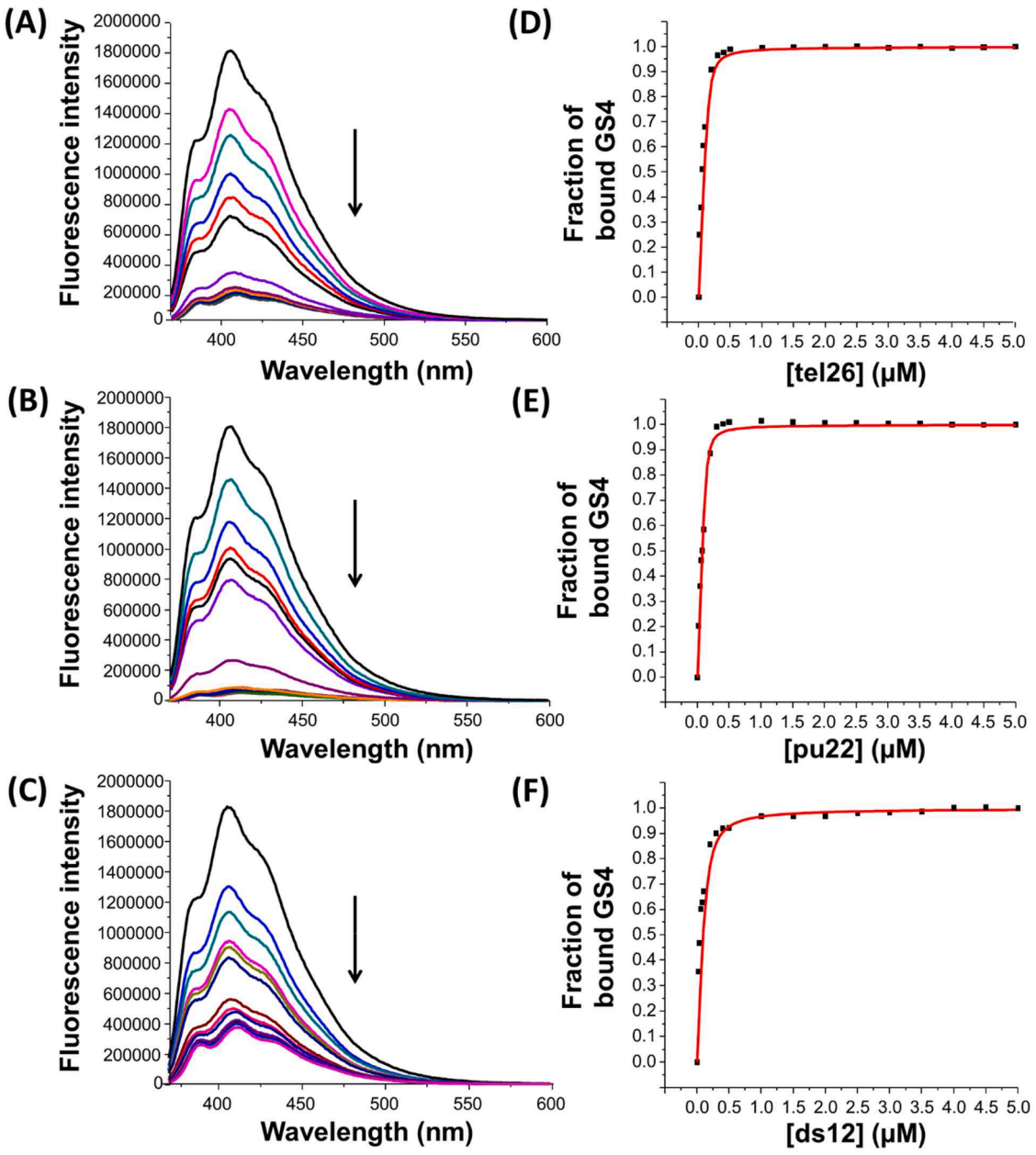

Fig. 6. Left panels: Fluorescence spectra obtained by adding increasing amounts of tel26 (A), pu22 (B) and ds12 (C) to solutions at a fixed concentration of **GS4** (2 μM). Arrows indicate the variation of fluorescence intensity on increasing DNA concentration. Right panels: Representative binding curves obtained by plotting the fraction of bound **GS4** to tel26 (D), pu22 (E) and ds12 (F) as a function of DNA concentration. The black squares represent experimental data; the red line represents the best fit obtained using an independent and equivalent-site model.

other hand, none of the investigated compounds produced any detectable change in the CD profile or structure stabilization of the control duplex.

The binding constants of the fluorescent ligands, *i.e.* **GS3, GS4** and **GS5**, with the DNA models were obtained by fluorescence spectroscopy measurements. Significant fluorescence quenching was observed upon titration of **GS3, GS4** and **GS5** with all three oligonucleotide models, but was however less marked in the case of the control duplex. From the comparison of the obtained K_b values, **GS4** emerged as the strongest but also the least selective G-quadruplex ligand in the series investigated by fluorescence spectroscopy titrations. In turn, **GS5** proved to be the most selective ligand for G-quadruplexes than duplex DNA. Furthermore, **GS5** showed higher affinity for the parallel G-quadruplex pu22 than for the hybrid G-quadruplex tel26, whereas **GS3** was found to be a stronger ligand of tel26 than of pu22.

Overall, the data obtained by the G4-CPG assay, CD and fluorescence spectroscopy demonstrated that the here investigated compounds, with the only exception of the naphthalene-based derivative **GS1**, were all able to strongly and selectively interact with telomeric and oncogenic G-quadruplexes, also discriminating the duplex DNA.

Additionally, molecular docking studies proved the ability of the here identified G-quadruplex-binding compounds to preferentially target the outer G-tetrads of both the hybrid tel26 and parallel pu22 G-quadruplexes. The binding pose based on asymmetrical stacking of the ligand cores on the tel26 G-tetrad allowed maximizing the interactions of one of the two pendant groups with the grooves, while in the symmetrical stacking of the ligand cores on the pu22 G-tetrad both substituents were close to the grooves with their interactions averaged. Moreover, it appeared that morpholine groups could be deeper accommodated in the G-quadruplex grooves than guanyl hydrazone or

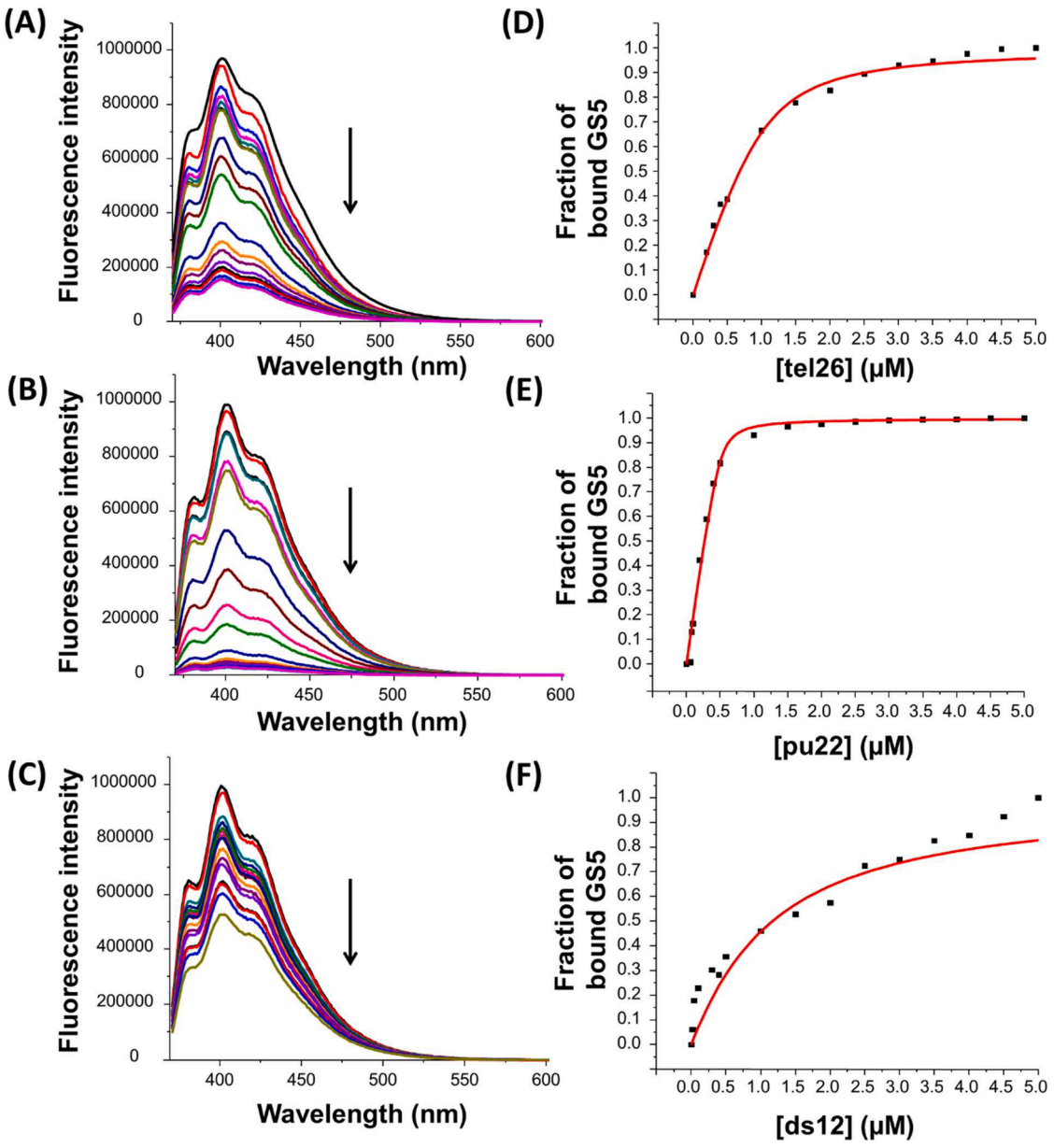

Fig. 7. Left panels: Fluorescence spectra obtained by adding increasing amounts of tel26 (A), pu22 (B) and ds12 (C) to solutions at a fixed concentration of **GS5** (2 μM). Arrows indicate the variation of fluorescence intensity on increasing DNA concentration. Right panels: Representative binding curves obtained by plotting the fraction of bound **GS5** to tel26 (D), pu22 (E) and ds12 (F) as a function of DNA concentration. The black squares represent experimental data; the red line represents the best fit obtained using an independent and equivalent-site model.

Table 3
Binding constants (K_b) for tel26, pu22 and ds12 in the presence of the investigated compounds measured by fluorescence experiments in 20 mM KCl, 5 mM potassium phosphate buffer (pH 7).

Compound	K_b (M^{-1})		
	tel26	pu22	ds12
GS3	5.3 (±1.8) x 10^6	1.7 (±0.5) x 10^6	4.4 (±0.4) x 10^5
GS4	5.8 (±1.8) x 10^6	8.4 (±2.3) x 10^6	2.3 (±1.0) x 10^6
GS5	2.8 (±0.8) x 10^6	5.1 (±1.8) x 10^6	2.1 (±0.3) x 10^5

piperazine groups.

Finally, **GS2, GS3, GS4** and **GS5** were investigated by preliminary *in vitro* cellular assays on human cancer cell lines, showing anti-proliferative activity in the low micromolar range that well correlates with their ability to target telomeric and oncogenic G-quadruplexes.

In conclusion, the obtained results suggested that a naphthalene moiety is not a valuable central scaffold to develop good ligands for telomeric/oncogenic G-quadruplex structures. On the other hand, modular and more flexible, non-fused polycyclic aromatic compounds based on bioxazoles appear to be very promising, if suitably decorated with pendant amino groups. In particular, the bioxazole derivative bearing piperazine groups on its lateral chains proved to be the most effective G-quadruplex ligand and the most active compound of the investigated series. On the other hand, bioxazole-based derivatives bearing morpholine groups on their lateral chains are endowed with higher telomeric/oncogenic G-quadruplex vs. duplex selectivity than bioxazole derivatives bearing piperazino or guanyl hydrazone groups.

Taken together, these data are very useful to evolve a series of optimized, second-generation G-quadruplex ligands based on bioxazole scaffolds, aiming at further improving their bioactivity and selectivity.

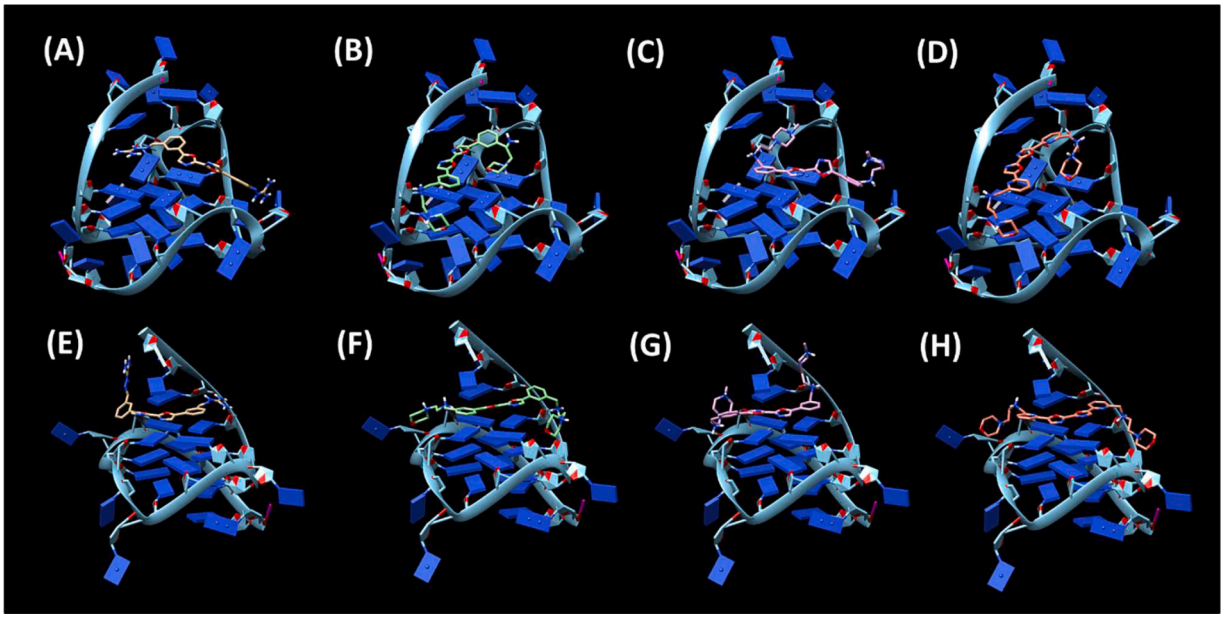

Fig. 8. Binding modes of **GS2, GS3, GS4** and **GS5** when docked to tel26 (A, B, C, D, respectively) and pu22 (E, F, G, H, respectively) G-quadruplexes. Ligands are represented as sticks (gray for **GS2**, green for **GS3**, purple for **GS4** and orange for **GS5**). 5′- and 3′-end of the G-quadruplexes are at the top and bottom, respectively, of each structure.

Table 4
IC_{50} values were established by testing increasing concentrations of each compound for 72 h on HeLa, MCF7 and HaCaT human cells by MTT assays.

Compound	IC_{50} (μM)		
	HeLa	MCF7	HaCaT
GS1	41	32	35
GS2	23	21	24
GS3	21	20	23
GS4	5	5	12
GS5	42	25	33

4. Materials and methods

4.1. Synthesis

4.1.1. General information

All employed reagents, including amines and isocyanides, are commercially available or synthesized according to literature procedures. Solvents were purchased in the anhydrous form and used without further purification. All the reactions were carried out under inert atmosphere, unless specified. ^{1}H NMR and ^{13}C NMR spectra were recorded using a Bruker AV 400 Ultrashield spectrometer. ^{1}H NMR and ^{13}C NMR chemical shifts were reported in parts per million (ppm) downfield from tetramethylsilane. Coupling constants (*J*) were reported in Hertz (Hz). The residual solvent peaks were used as internal references: ^{1}H NMR ($CDCl_3$ 7.26 ppm, DMSO-d_6 2.5 ppm), ^{13}C NMR ($CDCl_3$ 77.0 ppm, DMSO-d_6 39.5 ppm). In some ^{1}H NMR spectra performed in DMSO-d_6, signal of residual water appears as a broad singlet at 3.40 ppm. The following abbreviations were used to explain the multiplicities: *s* = singlet, *d* = doublet, *t* = triplet, *m* = multiplet, br = broad. IR spectra were recorded using a FT-IR 4700LE Jasco spectrometer and samples were prepared as KBr pellets (see Supporting Information). Mass spectra were recorded on a Thermo Fisher LCQ Fleet Ion Trap Mass Spectrometer equipped with UltiMate™ 3000 high-performance liquid chromatography (HPLC) system. HRMS spectra were obtained using Synapt G2-Si QTof mass spectrometer (Waters) with ZsprayTM ESI-probe for electrospray ionization (Waters). Chromatographic purifications were performed by Flash Chromatography (FC), using Merck Silica gel 60. Abbreviations: TosMIC = toluenesulfonylmethyl isocyanide, DMF = dimethyl formamide. To overcome solubility problems, some NMR spectra were recorded at 130 °C as indicated below.

4.1.2. Synthesis of naphthalene-2,7-dicarbaldehyde (1)

In a flame-dried round-bottom flask, 2,7-dibromonaphtalene (132 mg, 0.461 mmol, 1 eq) was dissolved in anhydrous THF (2.0 mL, 0.23 M) and the mixture was cooled to −78 °C. A solution of *n*-butyllithium (2.5 M in hexane, 1.25 mL, 6.8 eq) was added dropwise over 5 min, then the solution was stirred for 6 h at −78 °C. Anhydrous DMF (0.35 mL, 9.8 eq) was added dropwise over 2 min, then the reaction was warmed up at r.t., stirred for 5 min and quenched with distilled water (2.0 mL). The mixture was diluted with distilled water (30 mL) and extracted with DCM (3 × 30 mL). The combined organic phases were dried over anhydrous Na_2SO_4 and the solvent removed under reduced pressure. The crude product was purified by trituration with cold *n*-hexane to afford pure compound **1**; 70% yield; ^{1}H NMR (400 MHz, $CDCl_3$) δ 10.20 (s, 2H), 8.50 (s, 2H), 8.11 (d, J = 8.0 Hz, 2H), 8.01 (d, J = 8.0 Hz, 2H); ^{13}C NMR (100 MHz, $CDCl_3$) δ 192.3 (2C), 139.9, 135.9 (2C), 135.7 (2C), 132.7, 130.0 (2C), 126.7 (2C); HRMS (ESI) calcd for $C_{12}H_8O_2Na$ $[M+Na]^+$ 207.0422 found 207.0417.

4.1.3. Synthesis of 2,7-bis(1-(2-morpholinoethyl)-1H-imidazol-5-yl)naphthalene (GS1)

In a flame-dried round-bottom flask, compound **1** (88 mg, 0.478 mmol, 1 eq) and anhydrous $MgSO_4$ (141 mg, 4.4 eq) were suspended in a mixture of dry methanol and dry DMF (3:1 v/v, 2 mL, 0.24 M), then 4-(2-aminoethyl)morpholine was added dropwise (15 μL, 2.4 eq) and the mixture was refluxed for 2 h. K_2CO_3 (363 mg, 5.4 eq) and TosMIC (221 mg, 2.3 eq) were added in small portions over 1.5 h under vigorous stirring. The mixture was quenched by addition of H_2O and the aqueous phase was extracted with ethyl acetate (4 × 50 mL). The combined organic phases were dried over anhydrous Na_2SO_4 and the solvent removed under reduced pressure. The crude product was purified by flash chromatography (dichloromethane:methanol 90:10) to afford pure compound **GS1**; 34% yield; ^{1}H NMR (400 MHz, $CDCl_3$) δ 7.94 (d, J = 8.8 Hz, 2H), 7.86 (s, 2H), 7.76 (s, 2H), 7.54 (d, J = 8.4 Hz, 2H), 7.17 (s, 2H), 4.15 (t, J = 6.0 Hz, 4H), 3.61 (t, J = 4.4 Hz, 8H), 2.59 (t, J = 6.0 Hz, 4H), 2.36 (t, J = 4.8 Hz, 8H). ^{13}C NMR (100 MHz, $CDCl_3$) δ 139.6 (2C), 134.0

(2C), 133.4 (2C), 132.6 (2C), 129.3 (2C), 129.1 (2C), 128.4 (2C), 127.9 (2C), 67.5 (4C), 59.5 (2C), 54.3 (4C), 43.4 (2C); HRMS (ESI) calcd for $C_{28}H_{34}O_2N_6Na$ $[M+Na]^+$ 509.2641 found 509.2648.

4.1.4. 3,3′-([2,2′-bioxazole]−5,5′-diyl)dibenzaldehyde (3)

In a flame-dried round-bottom flask, compound **2** (143 mg, 0.841 mmol, 1 eq), $Pd(OAc)_2$ (17.6 mg, 0.1 eq), CuCl (15.9 mg, 0.2 eq), PPh_3 (41.0 mg, 0.2 eq) and $Cu(OAc)_2$ (112 mg, 0.75 eq) were dissolved in dry 1,4-dioxane (3.0 mL) and dry DMSO (0.3 mL). The reaction mixture was stirred at r.t. for 5 min, then was refluxed with an oil bath for 50 min. Successively, the reaction mixture was cooled to r.t., then was diluted with DCM (10 mL), filtered over a cotton pad, eluted with additional 100 mL of DCM and finally filtered again over cotton in order to remove the solid residues. The solvents were removed under reduced pressure to afford crude compound **3**, which was suspended in acetone (6.0 mL) and centrifuged. The supernatant was carefully removed, then the precipitate was resuspended in acetone (6.0 mL) and the process repeated two additional times. The precipitate was dried under reduced pressure to afford pure compound **3**; 50% yield; ^{1}H NMR (400 MHz, DMSO-d_6, 130 °C) δ 10.15 (s, 2H), 8.33 (s, 2H), 8.15 (d, J = 6.8 Hz, 2H), 8.03 (s, 2H), 7.98 (d, J = 6.8 Hz, 2H), 7.77 (t, J = 6.8 Hz, 2H); ^{13}C NMR (100 MHz, DMSO-d_6, 130 °C) δ 192.6 (2C), 152.0 (2C), 137.9 (4C), 130.6 (4C), 130.3 (2C), 128.3 (2C), 126.2 (2C), 125.8 (2C); HRMS (ESI) calcd for $C_{20}H_{12}O_4N_2Na$ $[M+Na]^+$ 367.0695 found 367.0688.

4.1.5. Synthesis of ((1Z,1′Z-[2,2′-bioxazole]−5,5′-diylbis(3,1-phenylene)bis(methanylylidene))bis(hydrazin-1-yl-2-ylidene))bis(aminomethaniminium) chloride (GS2)

In a round-bottom flask, compound **3** (21.3 mg, 0.0619 mmol, 1 eq) and aminoguanidine hydrochloride (13.3 mg, 1.9 eq) were suspended in absolute ethanol (4.0 mL, 0.01 M), then 3 drops of aqueous 1.0 M HCl were added and the mixture was refluxed for 6 h. The solvent was evaporated under reduced pressure to afford crude compound **GS2**, which was suspended in acetone (2.5 mL) and centrifuged. The supernatant was carefully removed, then the precipitate was resuspended in acetone (2.5 mL) and the process repeated twice. The precipitate was dried under reduced pressure to afford pure compound **GS2**; 61% yield; ^{1}H NMR (400 MHz, DMSO-d_6) δ 12.21 (s, 2H), 8.35 (s, 2H), 8.29 (s, 2H), 8.15 (s, 2H), 7.75–8.02 (m, 10H), 7.63 (t, J = 7.6 Hz, 2H); ^{13}C NMR (100 MHz, DMSO-d_6) δ 156.0 (2C), 152.2 (2C), 150.5 (2C), 146.4 (2C), 135.0 (2C), 130.2 (2C), 128.8 (2C), 127.6 (2C), 126.6 (2C), 126.0 (2C), 123.9 (2C); HRMS (ESI) calcd for $C_{22}H_{21}O_2N_{10}$ $[M+H]^+$ 457.1843 found 457.1850.

4.1.6. N,N′-([2,2′-bioxazole]-4,4′-diylbis(3,1-phenylene)bis(methylene))bis(2-morpholinoethan-1-amine) (GS3)

In a flame-dried round-bottom flask, compound **3** (45 mg, 0.131 mmol, 1 eq) and 4-(2-aminoethyl) morpholine (1.9 eq) were suspended in dry methanol (1.0 mL, 0.13 M) and the reaction mixture refluxed for 6 h. The solvent was removed under reduced pressure and the oily residue was dissolved in dry methanol (1.5 mL), then $NaBH_4$ (8.0 eq) was added in small portions over 2 min under vigorous stirring. The reaction mixture was heated at reflux for 1 h, then cooled down to r.t. and quenched with H_2O (25 mL). The aqueous phase was extracted with DCM (3 × 30 mL), then the combined organic phase were dried over anhydrous Na_2SO_4 and the solvent removed under reduced pressure. The crude product was purified by flash chromatography (dichloromethane:methanol 80:20) to afford pure **GS3;** 40% yield; ^{1}H NMR (400 MHz, $CDCl_3$) δ 7.76 (s, 2H), 7.67 (d, J = 7.6 Hz, 2H), 7.56 (s, 2H), 7.42 (t, J = 8.0 Hz, 2H), 7.36 (d, J = 7.6 Hz, 2H), 3.86 (s, 4H), 3.68 (t, J = 4.8 Hz, 8H), 2.72 (t, J = 6.4 Hz, 4H), 2.51 (t, J = 6.0 Hz, 4H), 2.41 (br t, 8H), 2.15–2.11 (m, 2H); ^{13}C NMR (100 MHz, $CDCl_3$) δ 153.7 (2C), 151.1 (2C), 142.1 (2C), 129.9 (2C), 129.8 (2C), 127.7 (2C), 125.2 (2C), 124.6 (2C), 124.2 (2C), 67.6 (4C), 58.8 (2C), 54.4 (4C), 54.3 (2C), 45.9 (2C); HRMS (ESI) calcd for $C_{32}H_{40}O_4N_6Na$ $[M+Na]^+$ 595.3009 found 595.3013.

4.1.7. N,N′-([2,2′-bioxazole]-4,4′-diylbis(3,1-phenylene)bis(methylene))bis(2-(4-methylpiperazin-1-yl)ethan-1-amine) (GS4)

This compound was synthesized following the same procedure described for **GS3** (Section 4.1.6) using 2-(4-methyl-piperazin-1-yl)-ethylamine instead of 4-(2-aminoethyl)morpholine; 26% yield; ^{1}H NMR (400 MHz, $CDCl_3$) δ 7.77 (br s, 2H), 7.69 (br d, J = 7.6 Hz, 2H), 7.57 (s, 2H), 7.43 (t, J = 8.0 Hz, 2H), 7.36 (d, J = 7.6, 2H), 3.87 (s, 4H), 2.73 (t, J = 6.9 Hz, 4H), 2.55–2.44 (m, 22 H), 2.28 (s, 6H); ^{13}C NMR (100 MHz, $CDCl_3$) δ 153.7 (2C), 151.1 (2C), 142.0 (2C), 129.9 (2C), 129.8 (2C), 127.7 (2C), 125.2 (2C), 124.7 (2C), 124.2 (2C), 58.2 (2C), 55.7 (4C), 54.3 (2C), 53.6 (4C), 46.5 (2C), 46.2 (2C); HRMS (ESI) calcd for $C_{34}H_{46}O_2N_8Na$ $[M+Na]^+$ 621.3641 found 621.3638.

4.1.8. N,N′-([2,2′-bioxazole]-5,5′-diylbis(pyridine-6,2-diyl)bis(methylene))bis(2-morpholinoethan-1-amine) (GS5)

This compound was synthesized following the same procedure described for **GS3** (Section 4.1.6) starting from compound **4** instead of compound **2**; 34% overall yield; ^{1}H NMR (400 MHz, $CDCl_3$) δ 7.93 (s, 2H), 7.78–7.76 (m, 4H), 7.34–7.32 (m, 2H), 3.98 (s, 4H), 3.71 (t, J = 4.4 Hz, 8H), 2.80 (t, J = 6.0 Hz, 4H), 2.56 (t, J = 5.6 Hz, 4H), 2.45 (br t, J = 4.0 Hz, 8H); ^{13}C NMR (100 MHz, $CDCl_3$) δ 160.5 (2C), 152.7 (2C), 150.8 (2C), 146.0 (2C), 137.4 (2C), 127.3 (2C), 122.3 (2C), 118.2 (2C), 67.1 (4C), 58.4 (2C), 55.0 (2C), 53.8 (4C), 45.7 (2C); HRMS (ESI) calcd for $C_{30}H_{38}O_4N_8Na$ $[M+Na]^+$ 597.2914 found 597.2919.

4.2. G4-CPG assay

Stock solutions (4 mM) for each compound were prepared by dissolving a known amount of the sample in pure DMSO. A defined volume was taken from the initial stock solution to obtain a 60 μM compound solution in 50 mM KCl, 10% DMSO, 10% CH_3CH_2OH aq. solution. The detailed general procedure adopted for the assays is as follows: weighed amounts of the nude CPG and G-quadruplex-/duplex-functionalized CPG supports (ca. 8 mg) [26] were left in contact with 300 μL of the compound solution in a polypropylene column (4 mL volume, Alltech) equipped with a polytetrafluoroethylene frit (10 μm porosity), a stopcock and a cap. After incubation on a vibrating shaker for 4 min, each support was washed with defined volumes of the washing solution (50 mM KCl, 10% DMSO, 10% CH_3CH_2OH aq. solution) or the releasing solution (2.5 M $CaCl_2$, 15% DMSO aq. solution or pure DMSO) and all the eluted fractions were separately analyzed by UV measurements. After treatment with the releasing solution, inducing G-quadruplexes and duplex denaturation, the supports were suspended in the washing solution and then subjected to annealing, by taking them at 75 °C for 5 min and then slowly cooling to r. t.

The UV measurements were performed on a JASCO V-550 UV–vis spectrophotometer. A quartz cuvette with a path length of 1 cm was used. The UV quantification of the compounds was determined by measuring the absorbance relative to the λ_{max} characteristic of each compound and referring it to the corresponding calibration curves. The errors associated with the % of bound ligand are within ± 2%.

4.3. Circular dichroism

CD spectra were recorded in a quartz cuvette with a path length of 1 cm, on a Jasco J-715 spectropolarimeter equipped with a Peltier-type temperature control system (model PTC-348WI). The spectra were recorded at 20 °C in the range 220–600 nm, 200 nm/min scanning speed and 2.0 nm bandwidth and were corrected by subtraction of the background scan with buffer. All the spectra were averaged over 3 scans. The oligonucleotides d[(TTAGGG)$_4$TT] (tel26), d(TGAGGGTGGGTAGGGTGGGTAA) (pu22) and d(CGCGAATTCGCG) (ds12) were purchased from Biomers as HPLC-purified compounds with a purity >99%. The oligonucleotides tel26 and ds12 were dissolved in a 20 mM KCl, 5 mM potassium phosphate buffer (pH 7), while pu22 was dissolved in a 10 mM Tris–HCl buffer (pH 7), to give 2 μM solutions, which were then

annealed by heating at 95 °C for 5 min, followed by slow cooling to r.t. CD titrations were obtained by adding increasing amounts of each compound (up to 2 molar equivalents, corresponding to a 4 μM compound solution) to the oligonucleotide solutions. For the CD melting experiments, the ellipticity was recorded at 290 nm for tel26, 263 nm for pu22 and 253 nm for ds12 with a temperature scan rate of 1 °C/min, in the range of 10–95 °C. Particularly, in CD experiments, pu22 was analyzed in a metal cation-free buffer considering that even in the presence of very low amounts of metal cations the pu22 G-quadruplex is so stable that its T_m value, as well as the related ΔT_m values in the presence of each ligand, cannot be accurately determined.

4.4. Fluorescence spectroscopy

Fluorescence spectra were recorded at 20 °C on HORIBA JobinYvon Inc. FluoroMax®−4 spectrofluorometer equipped with Peltier F-3004 Sample Heater/Cooler Peltier Thermocouple Drive, by using a quartz cuvette with a 1 cm path length. For the fluorescence titration experiments with **GS3, GS4** and **GS5** excitation wavelengths of 341, 342 and 337 nm were used, respectively. The spectra were recorded in the range 351–600 nm for **GS3**, 352–600 nm for **GS4** and 350–600 nm for **GS5**.

Titrations were carried out at a fixed concentration (2.0 μM) of each compound. Increasing amounts of tel26, pu22 and ds12 (up to 5 μM conc.) were added from 120 μM annealed stock solutions of each DNA sample dissolved in a 20 mM KCl, 5 mM potassium phosphate buffer (pH 7).

The fraction of bound ligand was calculated from the fluorescence intensity at 405 nm for **GS3**, 406 nm for **GS4** and 400 nm for **GS5**. The fraction of bound ligand was determined using the equation:

$$\alpha = \frac{Y - Y_0}{Y_b - Y_0}$$

where Y, Y_0 and Y_b are the values of fluorescence emission intensity at the maximum at each titrant concentration, at the initial and final state of the titration, respectively. These points were fitted with an independent and equivalent-sites model using the Origin 8.0 program [38].

The equation of the independent and equivalent-sites model is as follows:

$$\alpha = \left(\frac{1}{2[\mathrm{L}]_0}\right)\left\{\left([\mathrm{L}]_0 + n[\mathrm{DNA}] + \frac{1}{\mathrm{K_b}}\right) - \sqrt{\left([\mathrm{L}]_0 + n[\mathrm{DNA}] + \frac{1}{\mathrm{K_b}}\right)^2 - 4[\mathrm{L}]_0 \mathrm{n}[\mathrm{DNA}]}\right\}$$

where α is the mole fraction of ligand in the bound form, $[L]_0$ is the total ligand concentration, [DNA] is the added DNA concentration, n is the number of the equivalent and independent sites on the DNA structure and K_b is the binding constant.

4.5. Molecular docking

The G-quadruplex-forming oligonucleotides tel26 and pu22 were prepared using as starting point the NMR deposited structures of the complexes tel26/Auoxo6 (PDB 5MVB) and pu22/quindoline (PDB 2L7V), respectively, from which the bound ligands were removed. Molecular docking calculations were carried out using AutoDock Vina with the aid of its graphical user interface AutoDockTools [39,40]. The ligands and DNA targets were prepared by use of AutoDockTools and UCSF Chimera by assigning bond orders, adding hydrogen atoms and generating the appropriate protonation states. The ligands and targets were then converted to proper Autodock PDBQT file formats and the Gaisteiger charges were assigned. The 3D grid box dimensions were defined including the whole DNA macromolecules. The docking area was centered on the DNA center of mass and grid boxes of 110 Å × 100 Å × 80 Å and 100 Å × 90 Å × 60 Å for tel26 and pu22 G-quadruplexes, respectively, with a 0.375 Å spacing, were used. 100 docking poses were generated by using as docking parameters seed = random, exhaustiveness = 24 and number of binding modes = 20 for each of the 5 runs performed for each DNA/ligand system. Docking poses were clustered on the basis of their root-mean square deviation and ranked on the basis of binding energy. Molecular modeling figures were drawn by UCSF Chimera.

4.6. Biological assays

4.6.1. Cell cultures and cytotoxicity assays

Human HeLa CCL-2™ adenocarcinoma cells, human MCF7 breast cancer cells and immortalized human keratinocytes HaCaT were obtained from the American Type Culture Collection (ATCC, Manassas, VA, USA) and cultured in high-glucose Dulbecco's modified Eagle's medium (DMEM) supplemented with 10 % fetal bovine serum (FBS), 1% antibiotics (Pen/strep), and 1% L-glutamine at 37 °C in a humidified atmosphere containing 5% CO_2 as previously described [41]. To perform MTT assays, cells were seeded into 96-well plates at a density of 3×10^3 cells/well. After 24 h, cell supernatant was replaced with fresh medium containing increasing concentrations of the tested compounds. Subsequently, cells were cultured for different intervals of time (24, 48 and 72 h). After incubation, MTT assay was performed as previously described [42]. Briefly, cell culture supernatants were removed and cells were incubated with 0.5 mg/mL MTT reagent dissolved in DMEM medium without red phenol (100 μL/well). After 4 h of incubation at 37 °C, the resulting insoluble formazan salts were solubilized in anhydrous isopropanol containing 0.01 M HCl and quantified by measuring the absorbance at 570 nm by using an automatic plate reader spectrophotometer (Synergy H4 Hybrid Microplate Reader, BioTek Instruments, Inc., Winooski, VT). Cell viability was expressed as means of the percentage values obtained by comparison with control untreated cells.

4.6.2. Statistical analyses

Statistical analyses were performed by using a Student's *t*-Test. Significant differences were indicated as $^*P \leq 0.05$, $^{**}P \leq 0.01$, $^{***}P \leq 0.001$.

CRediT authorship contribution statement

Chiara Platella: Formal analysis, Investigation, Data curation, Writing – original draft, Writing – review & editing. **Andrea Citarella:** Formal analysis, Investigation, Writing – review & editing. **Marco Manenti:** Formal analysis, Investigation, Data curation, Writing – original draft, Writing – review & editing. **Guglielmo Spinelli:** Formal analysis, Writing – review & editing. **Rosa Gaglione:** Investigation, Writing – review & editing. **Angela Arciello:** Investigation, Writing – review & editing. **Claudia Riccardi:** Validation, Writing – review & editing. **Domenica Musumeci:** Validation, Validation, Writing – review & editing. **Daniela Montesarchio:** Writing – review & editing, Funding acquisition, Conceptualization. **Clelia Giannini:** Conceptualization, Validation, Writing – original draft, Writing – review & editing. **Alessandra Silvani:** Conceptualization, Data curation, Writing – review &

editing, Funding acquisition.

Declaration of Competing Interest

The authors declare that they have no known competing financial interests or personal relationships that could have appeared to influence the work reported in this paper.

Data availability

No data was used for the research described in the article.

Acknowledgments

Chiara Platella was supported by Fondazione Umberto Veronesi. The research leading to these results has received funding from AIRC under IG 2020 - ID. 25046 - P.I. Montesarchio Daniela. This research is part of the project "One Health Action Hub: University Task Force for the resilience of territorial ecosystems", supported by Università degli Studi di Milano–PSR 2021-GSA-Linea 6.

Supplementary materials

Supplementary material associated with this article can be found, in the online version, at doi:10.1016/j.molstruc.2023.137114.

References

[1] M.A. Zaimy, N. Saffarzadeh, A. Mohammadi, et al., New methods in the diagnosis of cancer and gene therapy of cancer based on nanoparticles, Cancer Gene Ther. 24 (6) (2017) 233–243, https://doi.org/10.1038/cgt.2017.16.
[2] L. Falzone, S. Salomone, M. Libra, Evolution of cancer pharmacological treatments at the turn of the third millennium, Front. Pharmacol. 9 (2018) 1300, https://doi.org/10.3389/fphar.2018.01300.
[3] C. Nakanishi, H. Seimiya, G-quadruplex in cancer biology and drug discovery, Biochem. Biophys. Res. Commun. 531 (1) (2020) 45–50, https://doi.org/10.1016/j.bbrc.2020.03.178.
[4] D. Varshney, J. Spiegel, K. Zyner, D. Tannahill, S. Balasubramanian, The regulation and functions of DNA and RNA G-quadruplexes, Nat. Rev. Mol. Cell Biol. 21 (8) (2020) 459–474, https://doi.org/10.1038/s41580-020-0236-x.
[5] K.V. Diveshkumar, S. Sakrikar, S. Harikrishna, V. Dhamodharan, P. I. Pradeepkumar, Targeting promoter G-quadruplex DNAs by indenopyrimidine-based ligands, ChemMedChem 9 (12) (2014) 2754–2765, https://doi.org/10.1002/cmdc.201402394.
[6] C. Platella, F. Ghirga, D. Musumeci, et al., Selective targeting of cancer-related G-quadruplex structures by the natural compound dicentrine, Int. J. Mol. Sci. 24 (4) (2023) 4070, https://doi.org/10.3390/ijms24044070.
[7] C. Platella, D. Capasso, C. Riccardi, D. Musumeci, M. Dellagreca, D. Montesarchio, Natural compounds from Juncus plants interacting with telomeric and oncogene G-quadruplex structures as potential anticancer agents, Org. Biomol. Chem. 19 (2021) 9953–9965, https://doi.org/10.1039/d1ob01995c.
[8] D. Monchaud, M.P. Teulade-Fichou, A hitchhiker's guide to G-quadruplex ligands, Org. Biomol. Chem. 6 (4) (2008) 627–636, https://doi.org/10.1039/b714772b.
[9] L. Savva, S.N. Georgiades, Recent developments in small-molecule ligands of medicinal relevance for harnessing the anticancer potential of G-quadruplexes, Molecules 26 (4) (2021), https://doi.org/10.3390/molecules26040841.
[10] A.R. Duarte, E. Cadoni, A.S. Ressurreição, R. Moreira, A Paulo, Design of modular G-quadruplex ligands, ChemMedChem 13 (9) (2018) 869–893, https://doi.org/10.1002/cmdc.201700747.
[11] J. Zhao, Q. Zhai, Recent advances in the development of ligands specifically targeting telomeric multimeric G-quadruplexes, Bioorg. Chem. 103 (2020), 104229, https://doi.org/10.1016/j.bioorg.2020.104229.
[12] C. Platella, S. Mazzini, E. Napolitano, et al., Plant-derived stilbenoids as DNA-binding agents: from monomers to dimers, Chem. Eur. J. 27 (2021) 8832–8845, https://doi.org/10.1002/chem.202101229.
[13] C. Platella, F. Ghirga, P. Zizza, et al., Identification of effective anticancer G-quadruplex-targeting chemotypes through the exploration of a high diversity library of natural compounds, Pharmaceutics 13 (2021) 1611, https://doi.org/10.3390/pharmaceutics13101611.
[14] A. Criscuolo, E. Napolitano, C. Riccardi, D. Musumeci, C. Platella, D. Montesarchio, Insights into the small molecule targeting of biologically relevant G-quadruplexes: an overview of NMR and crystal structures, Pharmaceutics 14 (11) (2022) 2361, https://doi.org/10.3390/pharmaceutics14112361.
[15] C. Platella, R. Gaglione, E. Napolitano, et al., DNA binding mode analysis of a core-extended naphthalene diimide as a conformation-sensitive fluorescent probe of G-quadruplex structures, Int. J. Mol. Sci. 22 (19) (2021) 10624, https://doi.org/10.3390/ijms221910624.
[16] S.M. Gowan, J.R. Harrison, L. Patterson, et al., A G-quadruplex-interactive potent small-molecule inhibitor of telomerase exhibiting in vitro and in vivo antitumor activity, Mol. Pharmacol. 61 (5) (2002) 1154–1162, https://doi.org/10.1124/mol.61.5.1154.
[17] D. Malpicci, S. Andolina, S. Di Ciolo, et al., Cyclic triimidazoles as stabilizers for gene promoter and human telomeric DNA G-quadruplexes, Eur. J. Org. Chem. (35) (2022), e202200718, https://doi.org/10.1002/ejoc.202200718.
[18] B. Zamiri, K. Reddy, R.B. Macgregor, C.E. Pearson, TMPyP4 porphyrin distorts RNA G-quadruplex structures of the disease-associated r(GGGGCC)n repeat of the C9orf72 gene and blocks interaction of RNAbinding proteins, J. Biol. Chem. 289 (8) (2014) 4653–4659, https://doi.org/10.1074/jbc.C113.502336.
[19] W.J. Chung, B. Heddi, M. Tera, K. Iida, K. Nagasawa, A.T. Phan, Solution structure of an intramolecular (3 + 1) human telomeric G-quadruplex bound to a telomestatin derivative, J. Am. Chem. Soc. 135 (36) (2013) 13495–13501, https://doi.org/10.1021/ja405843r.
[20] M.H. Hu, X.T. Lin, B. Liu, J.H. Tan, Dimeric aryl-substituted imidazoles may inhibit ALT cancer by targeting the multimeric G-quadruplex in telomere, Eur. J. Med. Chem. 186 (2020), 111891, https://doi.org/10.1016/j.ejmech.2019.111891.
[21] D. Verga, C.H. N'Guyen, M. Dakir, J.L. Coll, M.P. Teulade-Fichou, A Molla, Polyheteroaryl oxazole/pyridine-based compounds selected in vitro as G-quadruplex ligands inhibit rock kinase and exhibit antiproliferative activity, J. Med. Chem. 61 (23) (2018) 10502–10518, https://doi.org/10.1021/acs.jmedchem.8b01023.
[22] R.C. Monsen, J.O. Trent, G-quadruplex virtual drug screening: a review, Biochimie 152 (2018) 134–148, https://doi.org/10.1016/j.biochi.2018.06.024.
[23] J. Dai, M. Carver, L.H. Hurley, D. Yang, Solution structure of a 2:1 quindoline-c-MYC G-quadruplex: insights into G-quadruplex-interactive small molecule drug design, J. Am. Chem. Soc. 133 (44) (2011) 17673–17680, https://doi.org/10.1021/ja205646q.
[24] S. Mazzini, R. Gargallo, L. Musso, et al., Stabilization of c-KIT G-quadruplex DNA structures by the RNA polymerase I inhibitors BMH-21 and BA-41, Int. J. Mol. Sci. 20 (19) (2019) 4927, https://doi.org/10.3390/ijms20194927.
[25] J.W. Jaroszewski, V. Clausen, J.S. Cohen, O. Dahl, NMR investigations of duplex stability of phosphorothioate and phosphorodithioate DNA analogues modified in both strands, Nucleic Acids Res. 24 (5) (1996) 829–834, https://doi.org/10.1093/nar/24.5.829.
[26] C. Platella, D. Musumeci, A. Arciello, et al., Controlled pore glass-based oligonucleotide affinity support: towards high throughput screening methods for the identification of conformation-selective G-quadruplex ligands, Anal. Chim. Acta 1030 (2018) 133–141, https://doi.org/10.1016/j.aca.2018.04.071.
[27] V. Církva, P. Jakubík, T. Strašák, et al., Preparation and physicochemical properties of [6]helicenes fluorinated at terminal rings, J. Org. Chem. 84 (4) (2019) 1980–1993, https://doi.org/10.1021/acs.joc.8b02870.
[28] Q. Guo, L. Tao, C. Liu, et al., Orientation effects on C2(5)-C2'(5') linked bioxazole isomers synthesized via regioselective and sequential C[*sbnd*]H arylation, Chin. Chem. Lett. 32 (1) (2021) 425–428, https://doi.org/10.1016/j.cclet.2020.05.010.
[29] C. Platella, E. Napolitano, C. Riccardi, D. Musumeci, D. Montesarchio, Affinity chromatography-based assays for the screening of potential ligands selective for G-quadruplex structures, ChemistryOpen 11 (5) (2022), e202200090, https://doi.org/10.1002/open.202200090.
[30] D. Musumeci, J. Amato, A. Randazzo, et al., G-quadruplex on Oligo Affinity Support (G4-OAS): an easy affinity chromatography-based assay for the screening of G-quadruplex ligands, Anal. Chem. 86 (9) (2014) 4126–4130, https://doi.org/10.1021/ac500444m.
[31] A. Ambrus, D. Chen, J. Dai, T. Bialis, R.A. Jones, D. Yang, Human telomeric sequence forms a hybrid-type intramolecular G-quadruplex structure with mixed parallel/antiparallel strands in potassium solution, Nucleic Acids Res. 34 (9) (2006) 2723–2735, https://doi.org/10.1093/nar/gkl348.
[32] K. Guo, L. Hurley, D. Sun, Identification and characterization of nucleolin as a c-myc G-quadruplex-binding protein, J. Biol. Chem. 284 (35) (2009) 23622–23635, https://doi.org/10.1074/jbc.M109.018028.
[33] H.T. Le, M.C. Miller, R. Buscaglia, et al., Not all G-quadruplexes are created equally: an investigation of the structural polymorphism of the c-Myc G-quadruplex-forming sequence and its interaction with the porphyrin TMPyP4, Org. Biomol. Chem. 10 (47) (2012) 9393–9404, https://doi.org/10.1039/c2ob26504d.
[34] L. Petraccone, Higher-order quadruplex structures, Top. Curr. Chem. 330 (2013) 23–46, https://doi.org/10.1007/128_2012_350.
[35] P.D. Dans, L. Danilāne, I. Ivani, et al., Long-timescale dynamics of the Drew–Dickerson dodecamer, Nucleic Acids Res. 44 (9) (2016) 4052–4066, https://doi.org/10.1093/nar/gkw264.
[36] G. da Rosa, L. Grille, V. Calzada, et al., Sequence-dependent structural properties of B-DNA: what have we learned in 40 years? Biophys. Rev. 13 (2021) 995–1005, https://doi.org/10.1007/s12551-021-00893-8.
[37] J. Dai, M. Carver, C. Punchihewa, R.A. Jones, D. Yang, Structure of the hybrid-2 type intramolecular human telomeric G-quadruplex in K^+ solution: insights into

structure polymorphism of the human telomeric sequence, Nucleic Acids Res. 35 (15) (2007) 4927–4940, https://doi.org/10.1093/nar/gkm522.
[38] C. Giancola, B. Pagano, Energetics of ligand binding to G-quadruplexes, Top. Curr. Chem. 330 (2013) 211–242, https://doi.org/10.1007/128_2012_347.
[39] T. Oleg, J.O Arthur, AutoDock Vina: improving the speed and accuracy of docking with a new scoring function, efficient optimization, and multithreading, J. Comput. Chem. 31 (2010) 455–461, https://doi.org/10.1002/jcc.21334.
[40] A. Hospital, F. Battistini, R. Soliva, J.L. Gelpí, M. Orozco, Surviving the deluge of biosimulation data, Wiley Interdiscip. Rev. Comput. Mol. Sci. 10 (3) (2020) e1449, https://doi.org/10.1002/wcms.1449.
[41] R. Gaglione, G. Smaldone, R. Di Girolamo, R. Piccoli, E. Pedone, A. Arciello, Cell milieu significantly affects the fate of AApoAI amyloidogenic variants: predestination or serendipity? Biochim. Biophys. Acta - Gen. Subj. 1862 (3) (2018) 377–384, https://doi.org/10.1016/j.bbagen.2017.11.018.
[42] E. Dell'Olmo, R. Gaglione, A. Cesaro, et al., Host defence peptides identified in human apolipoprotein B as promising antifungal agents, Appl. Microbiol. Biotechnol. 105 (5) (2021) 1953–1964, https://doi.org/10.1007/s00253-021-11114-3.